Copper metallization of low-dielectric-constant a-SiCOF films for ULSI interconnects



2001 J. Phys.: Condens. Matter 13 6595

(http://iopscience.iop.org/0953-8984/13/31/301)

INSTITUTE OF PHYSICS PUBLISHING JOURNAL OF PHYSICS: CONDENSED MATTER

J. Phys.: Condens. Matter **13** (2001) 6595–6608 PII: S0953-8984(01)21601-4

# Copper metallization of low-dielectric-constant a-SiCOF films for ULSI interconnects

**Shi-Jin Ding[1], Qing-Quan Zhang[1], David Wei Zhang[1], Ji-Tao Wang[1] and Wei William Lee[2]**

[1] Department of Electronic Engineering, Fudan University, Shanghai 200433, China
[2] Taiwan Semiconductor Manufacturing Corporation (TSMC), Hsinchu, Taiwan, China

Received 1 February 2001
Published 19 July 2001
Online at stacks.iop.org/JPhysCM/13/6595

**Abstract**

The interactions between magnetron-sputtered Cu and plasma-enhanced chemical-vapour-deposited a-SiCOF film have been investigated via x-ray photoelectron spectroscopy (XPS), Auger electron spectroscopy (AES) and scanning electron microscopy (SEM). High-resolution C 1s, Cu 2p, O 1s, Si 2p and F 1s XPS spectra for the samples before and after annealing are collected. The results show that the C–Cu bond is not observed at the interface of Cu/a-SiCOF before or after the annealing. Moreover, the annealing causes the obvious shifts of Cu $2p_{3/2}$, C 1s, O 1s and Si 2p photoelectron peaks toward higher binding energy, and the underlying reasons are discussed in detail. The AES spectra of Cu $L_3M_{4,5}M_{4,5}$ with the etching time reveal that some chemical reactions take place at the interface during the sputtering deposition of copper on the a-SiCOF film, and possible reaction mechanisms are also presented. The Cu $2p_{3/2}$ XPS spectra and the SEM graphs demonstrate that the annealing enhances the interdiffusion between Cu and a-SiCOF film.

## 1. Introduction

As device dimensions decrease to sub-quarter micron, the smaller metal interconnection lines and narrower interline space induce an increase in the interconnection delay, expressed by $\tau = RC$, where $R$ and $C$ represent the resistance of the metal line and the capacitance of the interlayer insulator, respectively. Thus, although the speed of the device will increase as the feature size decreases, the interconnection delay becomes the major fraction of the total delay and limits the improvement in device performance [1]. For the sake of reducing the $RC$ delay, the use of low-dielectric-constant ($k$) dielectrics and low-resistivity metal is a way to limit the interconnection contribution to the delay. Among low-$k$ materials, amorphous carbon- and fluorine-doped silicon oxide (a-SiCOF) attracts more attentions because it shows a significant water resistivity, good thermal stability and adhesion on a silicon substrate, good electrical properties, a dielectric constant less than 2.5 etc [2–11]. Copper has been considered as a

  

substitute for Al interconnects in ULSI devices due to its low resistivity, high melting point, high mechanical strength and better electromigration resistance [12, 13]. Accordingly, in the interest of the integration of Cu and a-SiCOF dielectric into ULSI circuits, it is indispensable to investigate the interactions between them, such as chemical reactions occurring at the interface, mutual diffusion between them and so on. In the case of the copper metallization of low-$k$ materials, some papers have been published [14–17]. However, to our knowledge, the investigation of the interaction between Cu and a-SiCOF film has never been reported. In this paper, we investigate the interaction between magnetron-sputtered Cu and plasma-enhanced chemical-vapour-deposited a-SiCOF film using x-ray photoelectron spectroscopy (XPS), Auger electron spectroscopy (AES) and field emission scanning electron microscopy (FE-SEM).

## 2. Experiments

### *2.1. Deposition of a-SiCOF films*

The a-SiCOF films were deposited on clean Si substrates using a conventional parallel plate electrode plasma-enhanced chemical vapour deposition (PECVD) system. In the present study, the plasma was enhanced by a radio frequency (RF) of 13.56 MHz. The radio frequency power was fixed at about 150 W. The Si wafers were placed on the bottom electrode plate, which rotated at the speed of about 10 rpm in the interests of improving the temperature distribution on the bottom electrode and uniformity of the deposited film thickness. The substrate temperature was kept at about 100 °C. $C_4F_8$ and tetraethoxysilane (TEOS) were used as the feed gases, and introduced into the reaction chamber through separated mass flow controllers, respectively. Ar was used as the balance gas. All the films with a thickness of about 150 nm were deposited under the condition of 15 sccm TEOS, 25 sccm $C_4F_8$ and the total pressure of 70 Pa.

### *2.2. Deposition of copper films*

After the deposition of a-SiCOF film on the Si substrate, the sample was transferred into the sputtering chamber for the deposition of Cu film. The surface of a-SiCOF film was purged using Ar ion bombardment before copper deposition. Sputtering was performed at an rf power of 160 W and a working pressure of 0.3 Pa, Ar gas flow rate of 0.21 sccm. The sputtering target was a 99.99% Cu disc. Before deposition, the target was pre-sputtered for 1 min to remove any contaminate. The deposition rate was close to 0.1 nm per second. The thickness of the sputtering-deposited copper film was determined by sputtering time. In the present investigations, samples with a thickness of 0.5, 1, 20 and 30 nm Cu were obtained.

### *2.3. Characterization of the samples*

In order to observe the thermal behaviours of the samples, the samples were annealed at 450 °C for 30 min in 99.999% $N_2$. XPS spectra of the samples were collected on a Perkin-Elmer PHI 5000c ESCA system with standard Al K$\alpha$ radiation (1486.6 eV) at 93.90 eV of pass energy and low magnification. The base pressure of the test chamber was $10^{-9}$ Torr. All the binding energies were calibrated by using C 1s = 284.6 eV (neutral carbon peak) as a reference. Before the collection of XPS spectrum, a slight sputtering was applied to remove the adsorbed species on the surface of the sample, but it cannot remove the species bonded chemically with the surface. AES spectra of the sample was performed on an FE-AES system (Micro-Lab 310F, VG Scientific Co.) with an ion current of 1.0–1.1 $\mu$A, a detection area of about 0.1 mm$^2$ and

an ion energy of 10 keV. The surface microphotographs of the samples were observed with FE-SEM (Philips Company, model XL 30 FEG).

## 3. Results and discussion

### *3.1. XPS characterization*

XPS is a very sensitive probe of the atomic environment of a selected element. From XPS data it is possible to understand the role played by neighbouring bonded atoms because the exact value of the binding energy of the core electrons of a given element depends on its atomic surroundings [18]. That is, the energy of an electron in a tightly bound core state is determined by the attractive potential of the nuclei and the repulsive core Coulomb interaction with other electrons. When the chemical environment of a particular atom varies, which involves a spatial rearrangement of the valence charges of this particular atom and a different potential created by the nuclear and electronic charges on all the other atoms in the compound, the shift of the binding energy (so-called chemical shift) will take place.

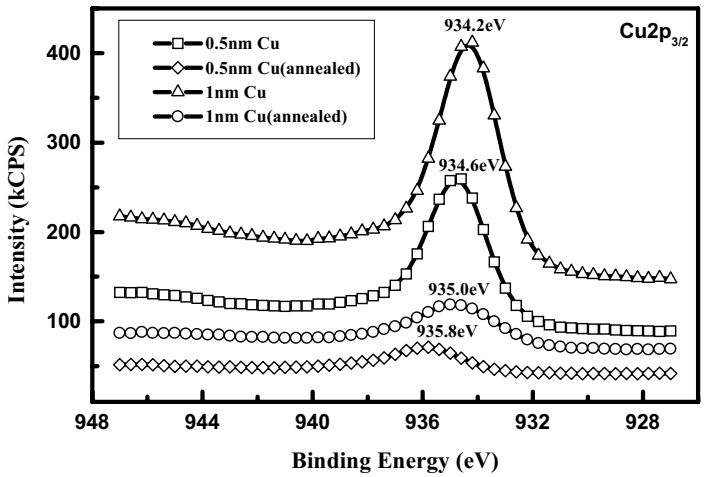


**Figure 1.** The high-resolution Cu $2p_{3/2}$ XPS spectra for the samples with different thicknesses of Cu before and after the annealing.

High-resolution Cu $2p_{3/2}$ XPS spectra are presented in figure 1. With the increase of Cu film thickness from 0.5 nm to 1 nm, the measured Cu $2p_{3/2}$ peak area increases, and the binding energy shifts from 934.6 eV to 934.2 eV. This manifests that the Cu $2p_{3/2}$ binding energy decreases with increasing copper coverage on the a-SiCOF film, which is in good accord with Carley and co-workers' observation [20]. However, in most publications the Cu $2p_{3/2}$ component is reported to have a binding energy of about 933 eV, such as 932.5 eV for 0.5 monolayers of copper evaporated on the Pd(111) surface [19], about 932.6 eV for metallic copper [21], 933.3 eV for low Cu concentrations ($\sigma_{Cu} = 5 \times 10^{13}$ cm$^{-2}$) [20]; as a result, in the present XPS spectra the shift of Cu $2p_{3/2}$ peak towards higher binding energy is more likely to result from charging effects. Of course, the difference between binding energies for a given peak also depends on the type of calibration of the spectrometer energy scale and the reference which is used for that. Here, it can be inferred that the shift due to the charging effect is approximate to 1.5 eV. On the other hand, it can be found that after the annealing the area of Cu $2p_{3/2}$ photoelectron peak for the sample with 0.5 nm or 1 nm Cu decreases. This indicates

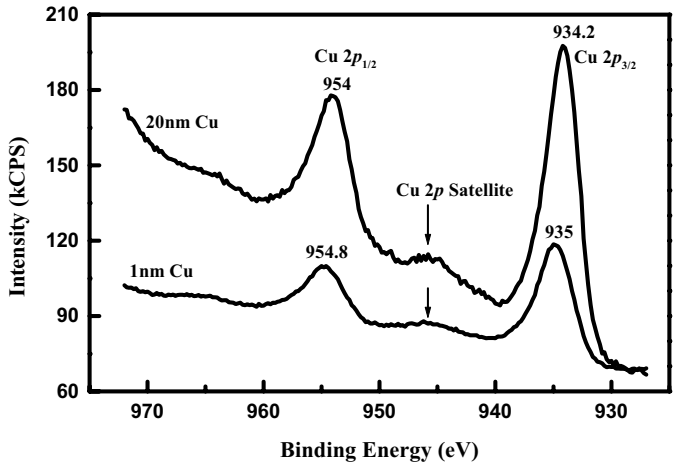


**Figure 2.** The Cu 2p XPS spectra for the annealed samples with different thicknesses of Cu.

that the annealing causes partial diffusion of Cu into the a-SiCOF films. Meanwhile, the Cu $2p_{3/2}$ peak moves towards higher binding energy, for example, from 934.6 eV to 935.8 eV for the sample with 0.5 nm Cu, and from 934.2 eV to 935 eV for that with 1 nm Cu. This perhaps results from a change in the chemical environment of copper. In addition, as the thickness of the deposited Cu film increases, the distortion of the Cu $2p_{3/2}$ core level shape is observed, which has been attributed to a very strong charging effect developing during Cu cluster formation by Rajagopal *et al* [14]. Figure 2 shows the Cu 2p XPS spectra for the annealed samples with different thicknesses of Cu. In the case of the sample with 1 nm Cu, two peaks corresponding to Cu $2p_{1/2}$ and $2p_{3/2}$ can be observed at 954.8 and 935 eV. As for the sample with 20 nm Cu, two peaks lie at 954 eV and 934.2 eV. Obviously, the Cu 2p peaks for the annealed sample with 20 nm Cu shift towards lower binding energy in comparison with the ones with 1 nm Cu. This also manifests that the binding energies of the Cu 2p core level are related to copper coverage, as mentioned before. According to Carley and co-workers' report that the Cu $2p_{3/2}$ binding energy for the bulk metallic copper is 932.8 eV [20], we can similarly deduce that the shift of the Cu $2p_{3/2}$ peak as a result of the charging effect is about 1.5 eV for the sample with 20 nm Cu. In addition, the appearance of a shakeup satellite around 946 eV suggests that the Cu(II) species is present at the surface [22]. Because copper is easily oxidized during its exposure to air, which will be discussed in section 3.2, it is possible that Cu(II) species results from an oxidation of Cu in air; meanwhile, for an ultra-thin copper film it maybe originates from a reaction between Cu and oxygen in an a-SiCOF film. Additionally, it is also found that for the samples with different thicknesses of Cu the binding energy difference between Cu $2p_{1/2}$ and Cu $2p_{3/2}$ core level remains constant at 19.8 eV. This suggests that the Cu element in the annealed samples is predominantly in one valence state [23], probably metallic copper, with only small amounts of Cu(II) species being present.

Considering the possibility of two chemical states of copper on the surface of the sample, the Cu $2p_{3/2}$ spectra for the sample with 1 nm Cu before and after annealing are deconvoluted into two Gaussian peaks, as shown in figure 3. In the case of the non-annealed sample, two peaks are located at 934.29 eV and 936.38 eV, respectively. If the shift of about 1.5 eV due to charging effect is taken into account, the actual binding energies corresponding to peaks 1 and 2 are respectively equal to about 932.79 eV and 933.88 eV, which are coincident with the published data, such as about 932.7 eV (metallic copper) and 933.7 eV (oxidized copper) [24],

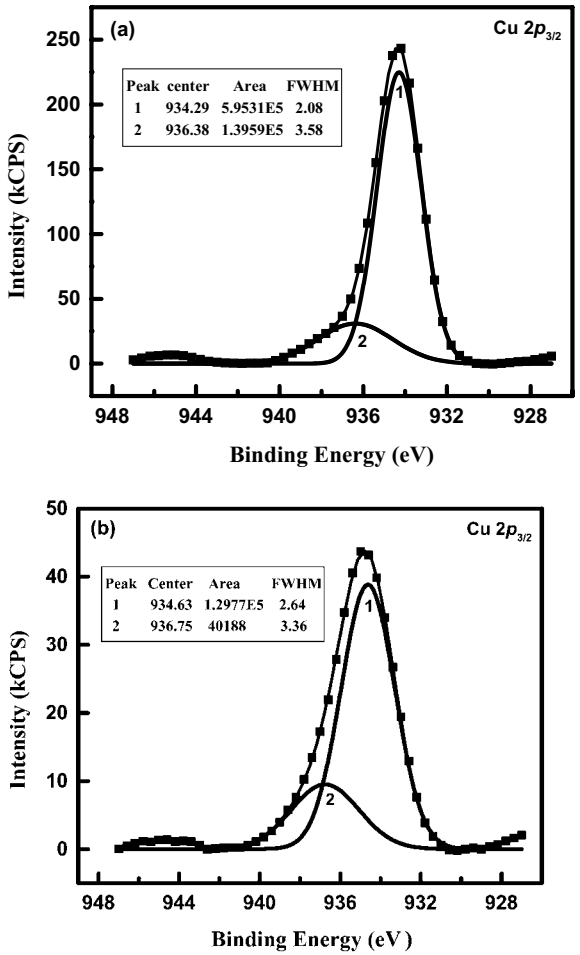


**Figure 3.** The deconvoluted Cu $2p_{3/2}$ spectra for (a) the non-annealed sample and (b) the annealed sample with 1 nm Cu.

932.7 eV (for copper metal and/or $Cu_2O$) and 933.6 eV (for CuO) [25], and about 932.6 eV (for metallic Cu and Cu(I) species) and 933.7 eV (for CuO species) [21]. It is helpful to be aware that the limited energy resolution of the XPS measurements poses limits in the possibility of disentangling chemically specific components. As a result, peak 2 with a full width at half maximum (FWHM) of 3.58 should be attributed to CuO, and peak 1 with a FWHM of 2.08 perhaps results from metallic Cu or Cu/$Cu_2O$. Here, it is worth emphasizing that a smaller FWHM for metals and a larger FWHM for oxides should be attributed to a greater vibrational broadening for the oxide [26]. According to the peak area, we can infer that the relative percentages of Cu or Cu/$Cu_2O$ and CuO in the non-annealed sample are about 76% and 24%, respectively. After the annealing, the area percentages of peaks 1 (934.63 eV) and 2 (936.75 eV) are respectively equal to about 81% and 19%. Meanwhile, the FWHM ratio of peak 1 to peak 2 increases to 0.78 in comparison with 0.58 for the non-annealed sample, which is perhaps due to the formation of more $Cu_2O$ after the annealing. In a word, in the non-annealed and annealed samples the metallic copper (or Cu/$Cu_2O$) is predominant, which is in accord with the conclusion deduced from the Cu 2p spectra. From figure 2 we can also

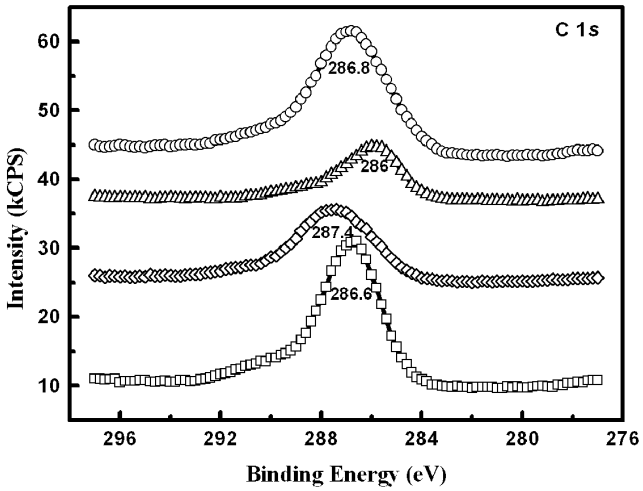


**Figure 4.** The high-resolution C 1s XPS spectra for the samples with different thicknesses of Cu before and after the annealing (squares and diamonds represent the non-annealed and annealed samples with 0.5 nm Cu; up triangles and circles represent the non-annealed and annealed samples with 1 nm Cu).

find that the intensity ratio of the Cu 2p satellite to the main Cu 2p line (Cu $2p_{3/2}$) is close to 20% for the annealed sample with 1 nm Cu. Nevertheless, for the annealed sample with 20 nm Cu the ratio decreases remarkably and is close to 7%. It can be considered that the annealing accelerates an interdiffusion between Cu and a-SiCOF, leading to the formation of more Cu oxides at the interface. However, compared with the sample with 1 nm Cu, the annealed sample with 20 nm Cu still has thicker Cu film which exceeds the detection depth of XPS apparatus, so the collected spectrum hardly stems from the interface. It goes without saying that the intensity ratio of the satellite to the Cu $2p_{3/2}$ line is smaller.

Figure 4 shows high-resolution C 1s XPS spectra. As the Cu thickness increases, the intensity of the C 1s peak decreases, especially for the annealed samples. Similarly, the annealing causes a shift of C 1s peak to higher binding energy, for instance, from 286.6 eV to 287.4 eV for the sample with 0.5 nm Cu, and from 286 eV to 286.8 eV for the sample with 1 nm Cu. In the interest of observing the influence of the annealing on chemical states of the carbon element, the C 1s spectra of the sample with 0.5 nm Cu before and after the annealing are deconvoluted, as indicated in figure 5. In the case of the C 1s spectrum before the annealing, four peaks with Gaussian distribution lie at 285.04, 286.72, 288.94 and 290.98 eV, and should be attributed to C–C or C–H contaminant, C–$CF_x$, C–F and $CF_2$ [27], accounting for about 1.3%, 77.8%, 15.5% and 5.4% on the basis of peak areas, respectively. The FWHM of about 2 eV is typical of the random-fragment molecular structure of plasma polymers, and certainly reflects the composite natures of the peaks [25]. After the annealing the C 1s spectrum is also fitted into four peaks (285.34, 287.09, 288.70 and 291.06 eV), corresponding to C–C or C–H contaminant, C–$CF_x$, C–F and $CF_2$ configurations, respectively. Evidently, the shift of the binding energy for C 1s core level electrons in each configuration occurs, and the $sp^3$ hybridized C–C bond increases. This indicates that the annealing results in a change in the chemical environment of carbon in the fluorocarbon embedded in the a-SiCOF film. From the F 1s XPS spectra we also find that the annealing causes loss of fluorine atoms, shown in figure 6. Thus, it is reasonable to think that the chemical shift induced by the annealing results not only from a change of carbon chemical environment due to breaking of C–F bonds, but also

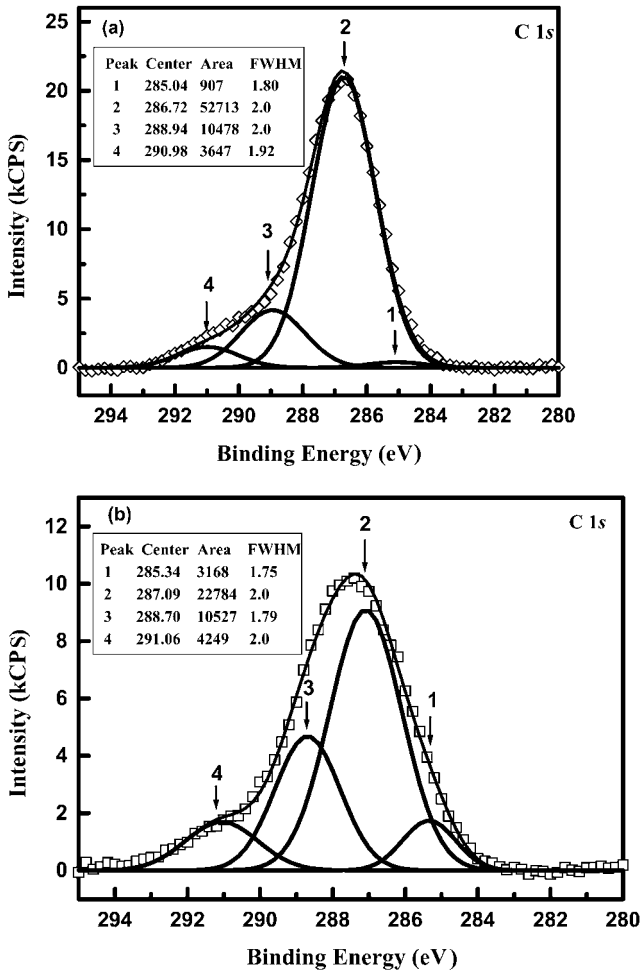


**Figure 5.** The deconvoluted C 1s spectra for (a) the non-annealed sample and (b) the annealed sample with 0.5 nm Cu.

from the film micro-structural difference invoked by Cu migration into a-SiCOF film, which will cause the solid state effect and the relaxation energy, as discussed in our previous paper [8]. In addition, from figure 4 we cannot observe any peak at binding energy less than 285 eV. According to [16, 17], the photoelectron peak of C 1s core level electrons for C–Cu is situated at about 283.6 eV. Therefore, it can be believed that the C–Cu bond cannot be formed during the deposition of the Cu film or even the annealing.

Figure 7 is the O 1s XPS spectra of the samples before and after the annealing. Obviously, before the annealing the peak area of the O 1s spectrum decreases with an increase in Cu film thickness. After annealing, the O 1s photoelectron peak moves from 533 eV to 535.2 eV for the sample with 0.5 nm Cu, and from 532.2 eV to 534.2 eV for that with 1 nm Cu. From figure 7 it can be found that the O 1s spectra are asymmetric, and should not be attributed to one peak. Therefore, the spectra are fitted with Gaussian distribution function. The deconvoluted spectra are shown in figure 8. In the case of the sample with 0.5 nm Cu, two peaks locating at 532.68 eV (peak 1) and 534.72 eV (peak 2) should be associated with copper oxide and

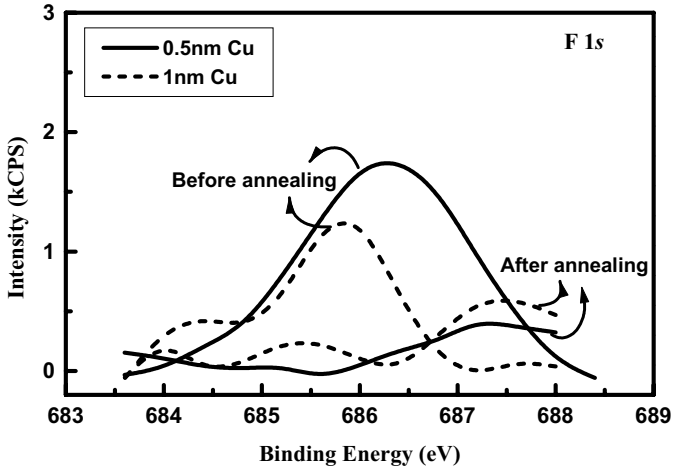


**Figure 6.** The high-resolution F 1s XPS spectra for the samples with different thicknesses of Cu before and after the annealing.

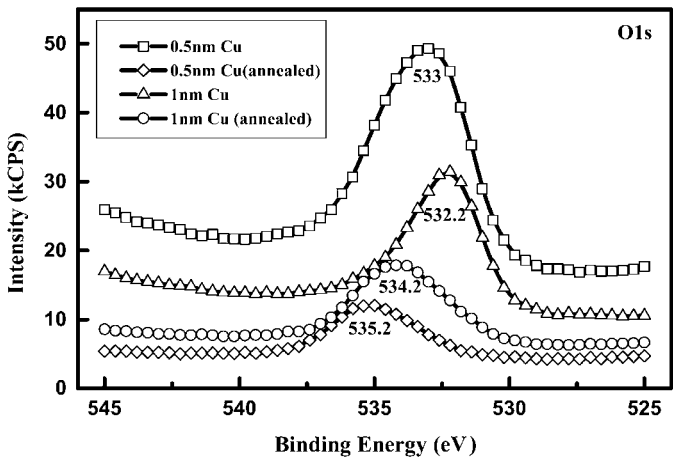


**Figure 7.** The high-resolution O 1s XPS spectra for the samples with different thicknesses of Cu before and after the annealing.

the oxygen element in the a-SiCOF film, which account for about 62% and 38%, respectively. As for the O 1s spectrum after the annealing, two peaks corresponding to copper oxide and a-SiCOF occur at 532.88 eV and 535.19 eV, and account for about 10% and 90%, respectively. This manifests that the annealing leads to a decrease in the percentage of copper oxide at the surface. It can be thought that the annealing enhances diffusion of copper and copper oxide into the a-SiCOF film, leading to an increase in the measured peak area of O 1s core level electrons from the a-SiCOF film.

Figure 9 reveals high-resolution Si 2p XPS spectra. As presented in Cu $2p_{3/2}$, C 1s, O 1s and F 1s spectra, the peak area of Si 2p core level electrons for the non-annealed samples decreases with increasing thickness of the Cu film. After the annealing, the Si 2p peak also exhibits a shift toward higher binding energy, i.e. from 104.8 to 106.4 eV for the sample with 0.5 nm Cu, and from 104.8 to 105.6 eV for the one with 1 nm Cu.

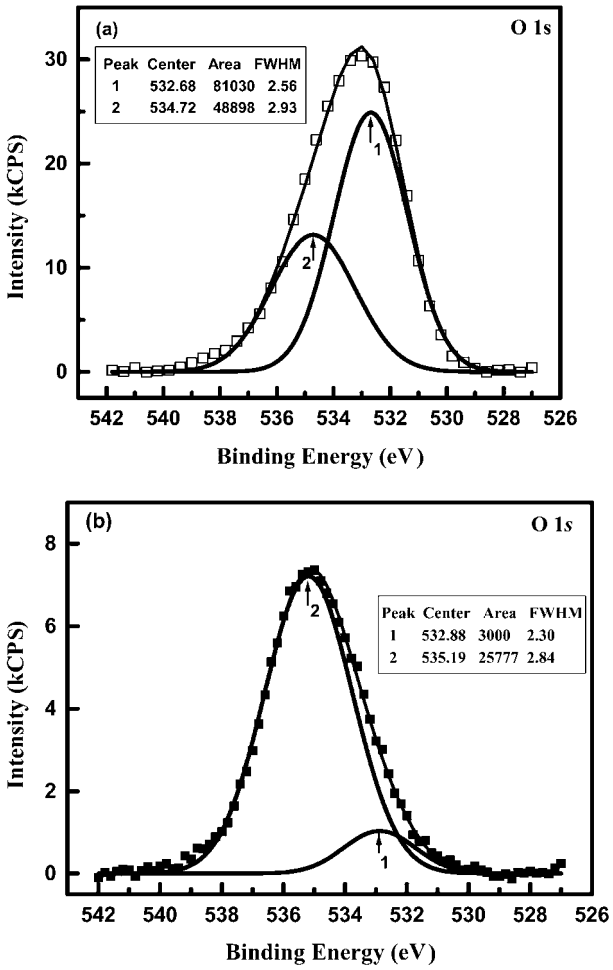


**Figure 8.** The deconvoluted O 1s XPS spectra for (a) the non-annealed sample and (b) the annealed sample with 0.5 nm Cu.

### *3.2. AES characterization*

The AES spectrum of the sample with 30 nm Cu is shown in figure 10. Obviously, we can observe a peak corresponding to OKVV at about 508 eV, which suggests that the oxidation of copper takes place at the surface, maybe leading to the formation of Cu(II) species. In addition, Auger peaks resulting from Cu $L_3M_{2,3}M_{2,3}$, $L_3M_{2,3}M_{4,5}$ and $L_3M_{4,5}M_{4,5}$ are also observed at about 765.5, 837.8 and 915.8 eV, respectively. The chemical shift of the Cu $L_3M_{4,5}M_{4,5}$ peak for the oxides compared to pure copper is a significant criterion to detect the oxidation state, provided the sample is conducting [28]. In the interests of understanding the oxidation state of Cu at the interface, the dependence of the Cu $L_3M_{4,5}M_{4,5}$ peak on etching time is presented in figure 11. When the etching time increases from 10 to 20 min, the Cu $L_3M_{4,5}M_{4,5}$ peak almost appears at the same position, i.e. about 918.11 eV. It can be believed that these peaks stem from pure copper. When the etching time increases to 23.6 min, the peak exhibits an obvious shift to lower kinetic energy, occurring at 916.64 eV. Takehiro *et al* reported that when metallic copper islands on a Pd (111) surface were exposed to $O_2$, the Cu LMM Auger line was shifted to lower

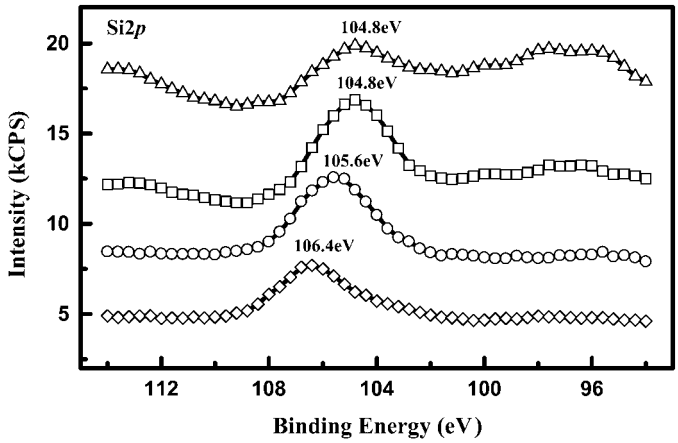


**Figure 9.** The high-resolution Si 2p XPS spectra for the samples with different thicknesses of Cu before and after the annealing (squares and diamonds represent the non-annealed and annealed samples with 0.5 nm Cu; up triangles and circles represent the non-annealed and annealed samples with 1 nm Cu).

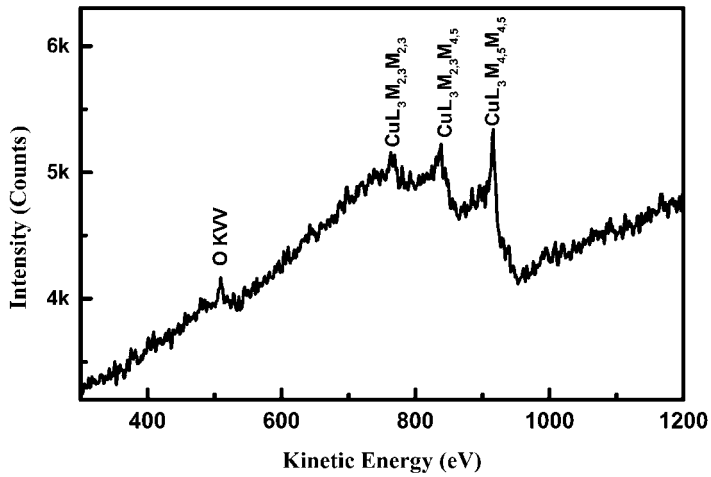


**Figure 10.** The AES for the sample of Cu(30 nm)/a-SiCOF.

kinetic energy (i.e. higher binding energy) [19]. Accordingly, we can believe that the shift of Auger peak in figure 11 is due to the oxidation of copper, which originates from the interface between Cu and a-SiCOF film. As the etching proceeds, the intensity of the peak decreases, indicating a reduction in copper concentration, and the peak becomes broad. Finally the peak evolves into two peaks perching at 914.74 and 917.83 eV respectively, and the intensity of the latter is higher than that of the former. This illustrates that some chemical reactions occur at the interface of Cu/SiCOF. Ma *et al* also declared that at the initial stages of Cu deposition on emeraldine base film of polyaniline, the Auger LMM signal at the kinetic energy of about 914.7 eV suggested the presence of Cu(I) species [21]. Therefore, the appearance of Auger peak at the kinetic energy of 914.74 eV indicates the formation of $Cu_2O$ at the interface, and the Auger signal at 917.83 eV may result from CuO.

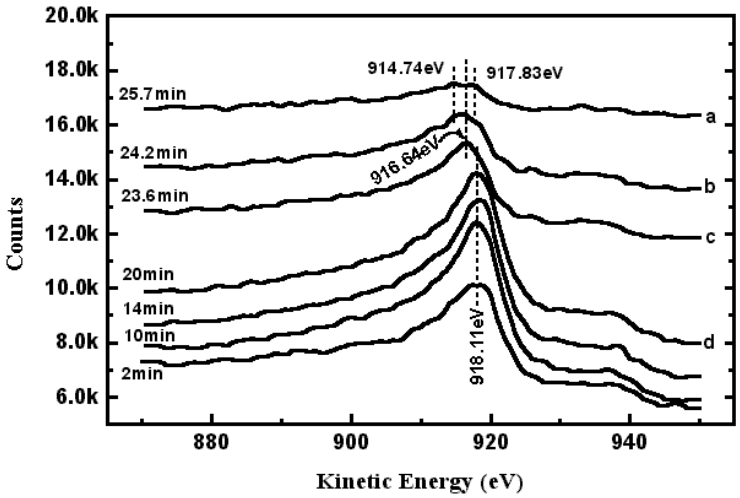


**Figure 11.** The dependence of AES for the sample of Cu(30 nm)/a-SiCOF on etching time.

As we know, the a-SiCOF film contains Si–F and Si–O bonds [6-10], and the bond energy of Si–O (108 kcal $mol^{-1}$) is smaller than that of Si–F (135 kcal $mol^{-1}$). Therefore, when energetic copper atoms deposit on the a-SiCOF film, the Si–O bond will break preferentially; subsequently the copper atom combines with oxygen, producing copper oxide. Consequently, possible reaction mechanisms at the interface are as follows. At the beginning of Cu sputtering deposition, CuO is formed because of the existence of a few copper atoms and a large number of oxygen atoms on the surface of a-SiCOF film. The reaction is expressed by $Cu + 2O \rightarrow O–Cu–O$. With the progress of Cu sputtering deposition, the amount of copper atoms on the a-SiCOF film increases and surpasses that of oxygen atoms. At this time, the reaction occurs as $2Cu + O \rightarrow Cu_2O$. Finally, when the amount of copper atoms exceeds that required for the above-mentioned reaction, the metallic copper then forms. The above-mentioned reaction mechanisms are in good agreement with the experimental observations. As shown by curve a in figure 11, at the initial stages of copper deposition we can observe the Auger signal of Cu(II) (i.e. CuO) at 917.83 eV besides that of Cu(I) (i.e. $Cu_2O$) at 914.74 eV, and the concentration of Cu(II) species is larger than that of Cu(I) species according to signal intensity. With the continuance of copper deposition, the intensity of Auger signal at about 914.7 eV increases and that at about 917.8 eV decreases, as expressed by curve b. This suggests an increase in the concentration of $Cu_2O$ and a decrease in that of CuO. When the etching time is equal to 23.6 min, as for curve c in figure 11, we can only observe one Auger signal at about 916.6 eV, which mainly results from $Cu_2O$. At the final stages of Cu deposition, the growth of copper film goes on, indicated by curve d.

### *3.3. SEM characterization*

Figure 12 is surface SEM graphs of the samples with 20 nm Cu. In the case of the non-annealed sample, small ball-like particles with a diameter of about 100 nm can be observed at the surface. As for the annealed sample, the surface becomes compact, and the ball-like particles become smaller. This is because the annealing is in favour of grain transmigration and re-growth. At the same time, we also find some defect clusters (i.e. small holes) at the surface of the sample, which testifies directly the diffusion of Cu into the a-SiCOF film as a

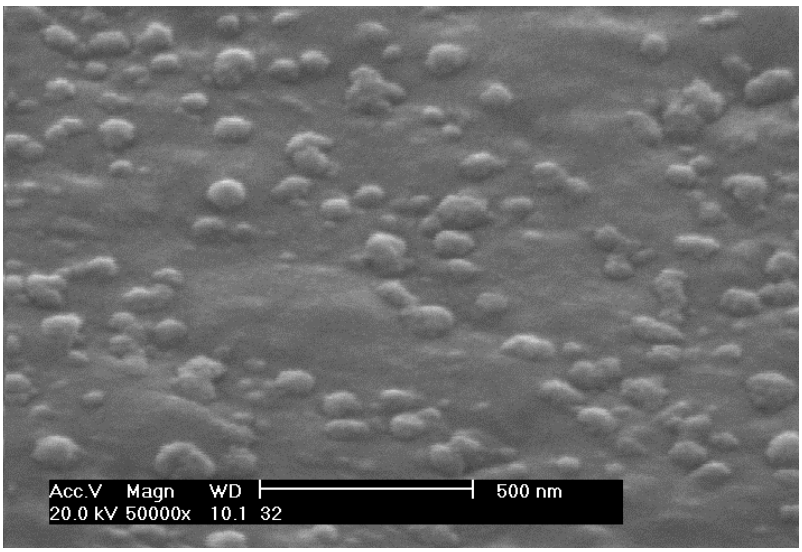


(a)

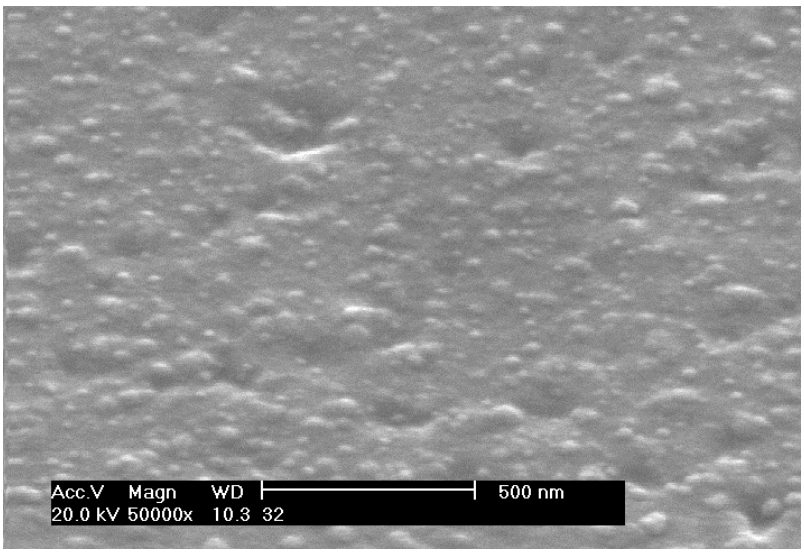


(b)

**Figure 12.** The SEM graphs for (a) the non-annealed sample and (b) the annealed sample with 20 nm Cu.

result of annealing. Although there is excellent adhesion between Cu and a-SiCOF by reason of the existence of chemical bonds like Cu-O, the notable diffusion created by the annealing will modify the effective thickness and permittivity of the interlayer dielectric, and even a short circuit maybe takes place. Accordingly, in the interests of the integration of Cu and a-SiCOF dielectric into ULSI, a diffusion barrier between them is required, such as Ta or TaN, which will be presented in another paper.

## 4. Conclusion

The interaction between sputtering-deposited copper and a-SiCOF film has been investigated with XPS, AES and SEM. With increasing thickness of Cu, the Cu $2p_{3/2}$ peak area increases gradually, and the peak areas of C 1s, O 1s, Si 2p and F 1s core level electrons decrease. Meanwhile, the Cu $2p_{3/2}$ peak moves to lower binding energy, which indicates that copper grains grow increasingly larger and become a continuous metallic-like film or larger metallic clusters. The annealing at 450 °C in $N_2$ results in the evident shifts of Cu $2p_{3/2}$, C 1s, O 1s and Si 2p peaks in the direction of higher binding energy. This should be attributed to a change of elemental chemical environment and the film micro-structural difference, causing the solid state effect and the relaxation energy. Moreover, the annealing decreases remarkably the intensities of the Cu $2p_{3/2}$ and F 1s peaks, suggesting a diffusion of copper into the a-SiCOF film and loss of fluorine. On the other hand, in the high-resolution C 1s spectra for the non-annealed and annealed samples we cannot observe any peak at binding energy less than 285 eV, revealing that the C–Cu bond is not produced at the interface of Cu/a-SiCOF. The AES spectra show that some copper is oxidized at the surface due to exposure to air. In addition, during the sputtering deposition of copper film the reactions between Cu and a-SiCOF occur. It can be considered that at the beginning of deposition CuO is formed; subsequently $Cu_2O$ will be produced. Finally, the growth of the metallic copper goes on. Directly, the SEM graphs illustrate that the annealing results in small holes at the surface of the sample. In brief, there is an excellent adhesion of copper on a-SiCOF film; however, a diffusion barrier between them is required in order to avoid the interdiffusion induced by the annealing.

## Acknowledgments

This project was supported by the National Natural Science Foundation of China (No 69776026) and the Foundation for University Key Teachers by the Ministry of Education of China.

## References

[1] Lee W W and Ho P S 1997 *MRS Bull.* **22** 19
[2] Lubguban J Jr, Saitoh A, Kurata Y, Inokuma T and Hasegawa S 1999 *Thin Solid Films* **337** 67
[3] Oh K S, Kang M S, Lee K M, Kim D S, Choi C K, Yun S M, Chang H Y and Kim K H 1999 *Thin Solid Films* **345** 45
[4] Lubguban Jr J, Kurata Y, Inokuma T and Hasegawa S 2000 *J. Appl. Phys.* **87** 3715
[5] Kim D S, Lee Y H and Park N H 1996 *Appl. Phys. Lett.* **69** 2776
[6] Ding S J, Chen L, Wan X G, Wang P F, Zhang D W and Wang J T *Mater. Chem. Phys.* at press
[7] Wang P F, Ding S J, Zhang D W, Zhang J Y, Wang J T and Lee W W 2001 *Appl. Phys.* A **72** at press
[8] Ding S J, Wang P F, Zhang D W, Wang J T and Lee W W 2001 *J. Phys. D: Appl. Phys.* **34** 155
[9] Wang P F, Ding S J, Zhang D W, Wang J T and Lee W W 2001 *Thin Solid Films* **385** 115
[10] Ding S J, Wang P F, Zhang W, Wang J T and Lee W W 2001 *Chin. Phys.* **10** 324
[11] Zhou Y Z, Qin S, Chan C and Chu P K 1998 *Mater. Res. Soc. Symp. Proc.* vol 511 (Pittsburgh, PA: Materials Research Society) p 63
[12] Nitta T, Ohmi T, Hsohi T, Sakai S, Sakaibara K, Imai S and Shibata T 1993 *J. Electrochem. Soc.* **140** 1131
[13] Wang H W, Chiou B S and Jiang J S 1999 *J. Mater. Sci.: Mater. Electron.* **10** 491
[14] Rajagopal A, Gregoire C, Lemaire J J, Pireaux J J, Baklanov M R, Vanhaelemeersch S, Maex K and Waeterloos J J 1999 *J. Vac. Sci. Technol.* B **17** 2336
[15] Labiadh A, Braud F, Torres J, Palleau J, Passemard G, Pires F, Dupuy J C, Dubois C and Gautier B 1997 *Microelectron. Eng.* **33** 369
[16] Popovici D, Klemberg-Sapieha J E, Czeremuszkin G, Sacher E, Meuniner M and Martinu L 1997 *Microelectron. Eng.* **33** 217

[17] Popovici D, Meuniner M and Sacher E *Electrochem. Soc. Proc.* **97/98** 44
[18] Zanatta A R and Chambouleyron I 1995 *Solid State Commun.* **94** 207
[19] Takehiro N, Yamada M, Tanaka K and Stensgaard I 1999 *Surf. Sci.* **441** 199
[20] Carley A F, Dollard L A, Norman P R, Pottage C and Roberts M W 1999 *J. Electron. Spectrosc. Relat. Phenom.* **98/99** 223
[21] Ma Z H, Tan K L, Chua W S, Kang E T and Neoh K G 2001 *Appl. Surf. Sci.* **173** 242
[22] Takano Y, Mori K, Koizumi K, Ozaki H and Sekizawa K 1998 *J. Alloys Compounds* **277** 447
[23] Khattak G D, Salim M A, Wenger L E and Gilani A H 2000 *J. Non-Cryst. Solids* **262** 66
[24] Li S, Kang E T, Neoh K G, Ma Z H and Tan K L 2000 *Surf. Sci.* **454–456** 990
[25] Silverstein M S, Sandrin L and Sacher E 2001 *Polymer* **42** 4299
[26] Sherwood P M A 1996 *J. Vac. Sci. Technol.* A **14** 1424
[27] Agraharam S, Hess D W, Kohl P A and Allen S A B 1999 *J. Vac. Sci. Technol.* A **17** 3265
[28] Timmermans B, Reniers F, Hubin A and Buess-Herman C 1999 *Appl. Surf. Sci.* **144/145** 54